CHEMISTRY OF MATERIALS
Article

Chem. Mater. **2009,** *21,* 5727–5742 5727
DOI:10.1021/cm9023875

Density Functional Theory Study of Ferrihydrite and Related Fe-Oxyhydroxides

Nathan Pinney,[†] James D. Kubicki,[§] Derek S. Middlemiss,[∥] Clare P. Grey,[∥] and Dane Morgan*[,†,‡]

[†]*Materials Science Program, University of Wisconsin—Madison, 201B Materials Science and Engineering Building, 1509 University Avenue, Madison, Wisconsin 53706-1595,* [‡]*Department of Materials Science and Engineering, University of Wisconsin—Madison, 244 Materials Science and Engineering Building, 1509 University Avenue, Madison, Wisconsin 53706-1595,* [§]*Department of Geosciences and Earth & Environmental Systems Institute, The Pennsylvania State University, University Park, Pennsylvania 16802, and* [∥]*Department of Chemistry, Stony Brook University, Stony Brook, New York 11794-3400*

Received August 3, 2009. Revised Manuscript Received October 10, 2009

The atomic and magnetic structure and thermodynamic stability of ferrihydrite (Fe_5O_8H) are calculated based on the structure recently proposed by Michel et al. (*Science* **2007**, *316*, 1726). Ferrihydrite stability is compared with that of the Fe-oxyhydroxide polymorphs goethite (α-FeOOH) and lepidocrocite (γ-FeOOH) and the oxide hematite (α-Fe_2O_3). The GGA+U method is employed to correct known errors in treating correlated d-electrons in Fe atoms. GGA+U yields smaller errors in calculated thermodynamic quantities relative to experiment as compared with a standard GGA functional for all of the Fe-oxyhydroxides studied. Good agreement is obtained between the DFT-predicted and experimental ferrihydrite structure when the effects of varying crystallinity and particle size are taken into account. The magnetic properties of ferrihydrite are modeled using a Heisenberg model parametrized with DFT-based magnetic coupling constants. The groundstate magnetic ordering of bulk ferrihydrite is predicted to be ferrimagnetic, with the Fe-site spins ordering with alternating alignment in layers stacked along the *c*-direction in the crystallographic unit cell. The groundstate is predicted to disorder to a paramagnetic structure at $T_N = 250$ K, undergoing a Néel transition. The enthalpy and Gibbs free energy of reaction of bulk crystalline ferrihydrite at 298.15 K are predicted to be $\Delta H^{298.15K}_{rxn}(Fe_5O_8H) = 6.4$ kJ/(mol-Fe) and $\Delta G^{298.15K}_{rxn}(Fe_5O_8H) = 6.9$ kJ/(mol-Fe), respectively, relative to bulk hematite and liquid water. The values demonstrate that fully crystalline ferrihydrite is metastable with respect to the formation of both hematite and goethite at 298.15 K but may be stabilized at small particle sizes due to favorably low surface formation energy. A simple surface energy model is used to predict the formation energy of ferrihydrite nanoparticles of arbitrary size, yielding results consistent with the observed formation energies for nanoparticle samples.

I. Introduction

Fe-oxyhydroxides and Fe-oxides are common minerals found in a wide range of environmental settings. They play an important role in the adsorption of contaminants (As, Sr, U, Cs, Pb, and Cd, among others) in groundwater systems and in the remediation and contaminant-plume control of acid mine tailings via adsorption or coprecipitation of heavy metals resulting from the processing of pyrite-containing metal ores and coals.[2] Their adsorptive properties are also important in industrial applications, for example, water treatment plants, wherein the contaminant heavy metals are either coprecipitated with or otherwise adsorbed by Fe-oxyhydroxide nanoparticles and disposed of as solid waste.[2] Given their environmental and industrial relevance, the basic materials properties of Fe-oxyhydroxides, including their structure and stability, are of considerable interest. However, the wide variety of often poorly crystalline polymorphs makes a simple description of the Fe-oxyhydroxide family an ongoing research challenge.

Often, the relative thermodynamic stabilities of the phases and polymorphic forms of Fe-oxyhydroxides differ by only a few kJ/mol,[3−5] and two or more phases are often observed in close association in natural environments having only slight gradients in temperature, moisture, oxygen, or contaminant availability.[2] Varying levels of surface and structural hydration, defect and dopant content, and widely varying particle sizes, ranging from less than 2 nm to micrometer-sized crystalline

*To whom correspondence should be addressed. E-mail: ddmorgan@wisc.edu.

(1) Michel, F. M.; Ehm, L.; Antao, S. M.; Lee, P. L.; Chupas, P. J.; Liu, G.; Strongin, D. R.; Schoonen, M. A. A.; Phillips, B. L.; Parise, J. B. *Science* **2007**, *316*(5832), 1726–1729.
(2) Cornell, R. M.; Schwertmann, U. *The iron oxides: structure, properties, reactions, occurrences and uses*, 2nd ed.; Wiley-VCH: Weinheim, 2003.
(3) Navrotsky, A.; Mazeina, L.; Majzlan, J. *Science* **2008**, *319*(5870), 1635–1638.
(4) Majzlan, J.; Grevel, K. D.; Navrotsky, A. *Am. Mineral.* **2003**, *88* (5−6), 855–859.
(5) Majzlan, J.; Navrotsky, A.; Schwertmann, U. *Geochim. Cosmochim. Acta* **2004**, *68*(5), 1049–1059.

Published on Web 11/12/2009

samples, complicate the thermodynamic landscape of this family of minerals.

An Fe-oxyhydroxide of particular interest is ferrihydrite, a common material in groundwater, surface and near-surface waters, sediment, and soil environments,[2] whose small size (typically 2−7 nm) and poor crystallinity render crystal structural determination challenging.[6−10] Samples of natural or synthetic ferrihydrite are usually characterized by the number of discernible broad X-ray diffraction peaks. The most common synthetic types are two-line and six-line ferrihydrite, manifesting two and six broad and poorly resolved diffraction peaks, respectively. Better-resolved diffraction peaks are generally associated with higher crystallinity (lower structural disorder) and larger particle sizes, properties that tend to occur together.[8,9,11,12] Previous structural models for ferrihydrite have suggested a multiphase system based on the hexagonal packing of oxygen atoms, which incorporates both defected and defect-free phases (the d- and f-phases, respectively), and includes variable amounts of nanocrystalline hematite, maghemite/magnetite, and/or highly defective material.[6,8−12] These models do not propose specific atomic positions, especially for structural H_2O groups or H atoms, and also propose random alternation of oxygen stacking arrangements[6] and random Fe occupancies in both d- and f-phases.[9] Poorly determined atomic positions and multiphase nanoscale systems with significant interfaces present considerable obstacles for current DFT methods, which, in terms of computational tractability, are limited to systems of the order of hundreds of atoms and cannot easily locate optimal complex structures without an estimate for initial atomic coordinates. Michel et al.[1] in 2007 proposed a single-phase crystal structure for ferrihydrite with uniquely defined positions for all the atoms (although with partial Fe occupancies and no information on H positions, the treatment of which is discussed further below), making the new structure better suited for DFT studies.

The goal of the current work is to use solid-state DFT calculations to explore the structure and energetics of and magnetic coupling within the newly proposed ferrihydrite structure and to assess the application of GGA+U methods to the Fe-oxyhydroxide materials. To estimate the accuracy of the calculations, we performed a thorough comparison of GGA+U energetics with experimental data for the major Fe-oxyhydroxide materials. In the case of ferrihydrite, however, a number of different aspects must first be considered during the construction of a satisfactory ab initio model.

First, the atomic positions and lattice parameters for ferrihydrite are predicted and compared to the experimental data for defected nanoparticles. This requires that the H positions, not determined in the experimental structure, be identified as described in Section IV.A.

Second, the correct magnetic ground state must be used for accurate DFT energy calculations, but the ferrihydrite bulk magnetic structure is currently unknown. Thus, in Section IV.B, a DFT-based magnetic model is constructed for bulk crystalline ferrihydrite, which is then used in the following calculations. Finally, having developed and, where possible, validated the DFT atomic and magnetic structural models for ferrihydrite, the computed energetics are compared with experimental values in Section IV.C.

Considering the small experimentally measured relative stabilities separating the Fe-oxyhydroxides structures,[3−5] every effort must be made to obtain accurate DFT values. In particular, the GGA+U method is used to treat Fe d-electron correlation effects, and it is shown that the introduction of the strong on-site Coulomb and exchange interactions, represented by the Hubbard U parameter, reduces errors in Fe-oxyhydroxide energies and relative stabilities significantly (Section IV. C). For example, GGA calculations used to obtain the stability of goethite and lepidocrocite relative to hematite+water give errors of 9.5 and 24.8 kJ/(mol-Fe) respectively, compared to experiment, whereas optimal GGA+U calculations give errors of only −1.7 and 2.1 kJ/(mol-Fe), respectively. We then develop a thermodynamic model for Fe-oxide and -oxyhydroxide relative stability that includes treatment of the water reference state, zero point H vibrational energies, and corrections for thermal excitations and nanoparticle effects. Analogous calculations on isostructural Al-oxyhydroxides, which are somewhat simpler due to the absence of magnetic and correlated d-electron effects, are also used to validate the thermodynamic model. Taken together, these results help assess the Michel model, improve our understanding of the complex ferrihydrite structure, and provide a validated computational approach for studying Fe-oxyhydroxides with GGA+U methods.

II. Properties of Fe-Oxyhydroxide Materials

Multiple common Fe-oxyhydroxide compounds[2] contain Fe^{III} cations on a variety of oxygen/hydroxyl anion arrangements (Table 1). Goethite (α-FeOOH) and hematite (α-Fe_2O_3) are generally considered the most stable forms as bulk crystalline solids under atmospheric conditions. Lepidocrocite (γ-FeOOH) and ferrihydrite (nominally Fe_5O_8H)[1] are typically thought to be less stable as fully crystalline structures but may be stabilized as small particles, due to their relatively low surface enthalpy.[3] Ferrihydrite often forms as a metastable precursor phase as the kinetic product of rapid precipitation of Fe^{III} hexa-aquo ion $Fe^{III}(OH_2)_6^{3+}$ in solution, which then transforms over time into one of the more stable phases (typically goethite or hematite).[2]

(6) Manceau, A. *Clay Minerals* **2009**, *44*, 19–34.
(7) Rancourt, D. G.; Meunier, J. F. *Am. Mineral.* **2008**, *93*(8−9), 1412–1417.
(8) Janney, D. E.; Cowley, J. M.; Buseck, P. R. *Am. Mineral.* **2000**, *85* (9), 1180–1187.
(9) Janney, D. E.; Cowley, J. M.; Buseck, P. R. *Am. Mineral.* **2001**, *86* (3), 327–335.
(10) Jansen, E.; Kyek, A.; Schafer, W.; Schwertmann, U. *Appl. Phys. A: Mater. Sci. Process.* **2002**, *74*, S1004–S1006.
(11) Drits, V. A.; Sakharov, B. A.; Salyn, A. L.; Manceau, A. *Clay Minerals* **1993**, *28*(2), 185–207.
(12) Janney, D. E.; Cowley, J. M.; Buseck, P. R. *Clays Clay Minerals* **2000**, *48*(1), 111–119.

Table 1. Isostructural Fe- and Al-Oxyhydroxides

Fe-based structure	Al-based analogous stucture
hematite, α-Fe_2O_3	corundum, α-Al_2O_3
goethite, α-FeOOH	diaspore, α-AlOOH
lepidocrocite, γ-FeOOH	boehmite, γ-AlOOH
ferrihydrite, Fe_5O_8H	akdalaite, Al_5O_8H
$Fe(OH)_3$ structural analog unknown	gibbsite, $Al(OH)_3$

Other relatively common FeOOH and Fe-oxide polymorphs are not included in this study due to uncertainties in their crystal structure or chemical composition. Specifically, akaganéite (β-FeOOH) is excluded due to the presence of the Cl^- anion in the crystal structure, which complicates the thermodynamic analysis by requiring an additional reference state for Cl. Maghemite (γ-Fe_2O_3) and magnetite (Fe_3O_4) are also important structures in the Fe-oxyhydroxide family but are excluded due to random Fe-vacancy ordering in the former and the presence of mixed Fe^{II} and Fe^{III} sites in the latter; both of these conditions add considerable complexity to a rigorous DFT investigation. Therefore, this work will focus on hematite, goethite, lepidocrocite, and ferrihydrite, with a particular focus on the recently proposed structure of ferrihydrite.

The three Fe-oxyhydroxide materials studied (goethite, lepidocrocite, ferrihydrite) can be formed, at least with respect to stoichiometry, from a combination of hematite and water:

$$Fe_2O_3 + H_2O \rightarrow (Fe_2O_3)\cdot H_2O \rightarrow 2(FeOOH) \quad (1)$$

$$5(Fe_2O_3) + H_2O \rightarrow 5(Fe_2O_3)\cdot H_2O \rightarrow 2(Fe_5O_8H) \quad (2)$$

Equation 1 is for goethite and lepidocrocite while eq 2 is for ferrihydrite. Here the ferrihydrite stoichiometry is assumed to be that given in the Michel model.[1] The single-phase crystalline Michel model is based on the hexagonal $P6_3mc$ space group and incorporates Fe atoms in both octahedral (80% of Fe sites) and tetrahedral (20% of Fe sites) O coordinations. Fe atoms are arranged in layers perpendicular to the crystallographic *c*-axis (Figure 1), occupying three symmetry-distinct sites, referred to as Fe1, Fe2, and Fe3, matching the convention of the original Michel reference.[1] The Fe1 sites comprise edge-sharing Fe-octahedra forming layers consisting exclusively of Fe1. These layers are separated by a mixed layer of octahedrally coordinated Fe2 sites (which occupy a different Wyckoff symmetry position and have slightly different Fe−O bonding geometries than the Fe1 octahedra) and tetrahedrally coordinated Fe3 sites. The Michel model incorporates many structural features akin to magnetite, including the mixed tetrahedral and octahedral coordination of Fe. However, in contrast with magnetite, no ferrous iron is expected in ferrihydrite.

Important for comparison in the study of the Fe-oxyhydroxide materials are the isostructural Al-oxyhydroxide

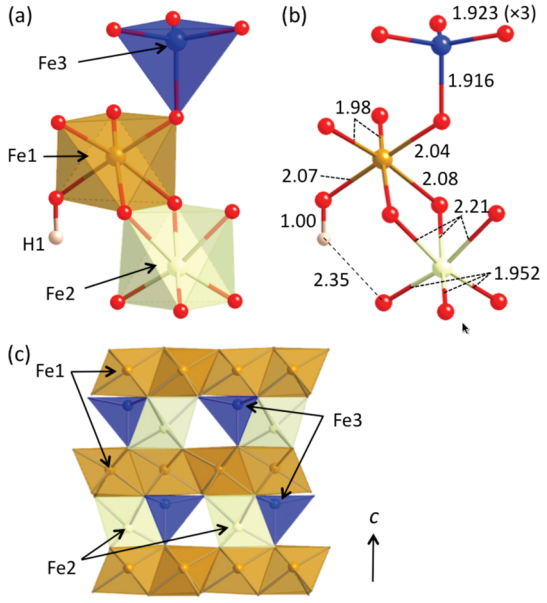

Figure 1. DFT-optimized Michel et al. ferrihydrite structure including H atoms (initial positions taken from akdalaite structure[18]). The structure has three symmetry-distinct Fe atoms (a) in the primitive cell, Fe1 (brown) (greyscale: medium gray) and Fe2 (white) (greyscale: light gray) are octahedrally coordinated by six oxygen atoms each (red) (greyscale: dark gray, polyhedral corners), Fe3 (blue) (greyscale: black) is tetrahedrally coordinated. Calculated bond lengths (Å) are shown in part (b). Part (c) shows the layering arrangement of Fe1 and mixed Fe2/Fe3 layers.

materials (Table 1) that form under relatively similar conditions and display roughly similar stability relationships.[13] Calculations based on the isostructural Al-based materials are arguably simpler, as they lack the additional complications arising from magnetic and d-electron correlation effects. Thus, the pure DFT-based thermodynamics computed for Al materials might effectively serve as a benchmark for the more technically complex Fe-containing materials. Note that the Michel ferrihydrite structure is isostructural (at least up to the H positions, which were not given) with the Al-based material akdalaite.

III. Methodology

This section describes the basic computational methods used to perform the DFT calculations (Section III.A) and the theoretical background for the finite temperature thermodynamics used to compare the ab initio and experimental Fe-oxyhydroxide energetics (Section III.B). The thermodynamic theory is applied in Section IV.C.

A. Computational Methods. Calculations were performed using density functional theory (DFT) and the projector-augmented wave (PAW) method,[14,15] with the Vienna Ab-initio Simulation Package (VASP).[16] Exchange-correlation was treated in the generalized gradient approximation (GGA), as parametrized by Perdew, Burke, and Ernzerhof (PBE).[17] The following valence

(13) McHale, J. M.; Navrotsky, A.; Perrotta, A. J. *J. Phys. Chem. B* **1997**, *101*(4), 603–613.
(14) Kresse, G.; Joubert, D. *Phys. Rev. B* **1999**, *59*(3), 1758–1775.
(15) Blochl, P. E. *Phys. Rev. B* **1994**, *50*(24), 17953–17979.
(16) Kresse, G.; Furthmuller, J. *Phys. Rev. B* **1996**, *54*(16), 11169–11186.
(17) Perdew, J. P.; Burke, K.; Ernzerhof, M. *Phys. Rev. Lett.* **1996**, *77* (18), 3865–3868.
(18) Anisimov, V. I.; Aryasetiawan, F.; Lichtenstein, A. I. *J. Phys.: Condens. Matter* **1997**, *9*(4), 767–808.

Table 2. Fe/Al-Oxyhydroxide Structural Information and Experimental (Calculated) Unit Cell Dimensions

structure	formula	space group	*a*, Å	% error	*b*, Å	% error	*c*, Å	% error	ref
hematite	α-Fe_2O_3	$R\bar{3}c$	5.03 (5.08)	0.8	5.03 (5.08)	0.8	13.75 (13.95)	1.4	2
goethite	α-FeOOH	*Pnma*	9.96 (10.05)	0.9	3.02 (3.06)	1.3	4.61 (4.63)	0.4	2
lepidocrocite	γ-FeOOH	*Bbmm*	3.07 (3.09)	0.7	12.52 (12.48)	−0.3	3.87 (3.95)	2.1	2
ferrihydrite	Fe_5O_8H	$P6_3mc$	5.93 (5.99)	1.0	5.93 (5.99)	1.0	9.13 (9.35)	2.4	1
corundum	α-Al_2O_3	$R\bar{3}c$	5.12 (5.18)	1.1	5.12 (5.18)	1.1	5.12 (5.18)	1.1	25
diaspore	α-AlOOH	*Pbnm*	4.40 (4.41)	0.2	9.43 (9.48)	0.5	2.85 (2.88)	1.0	26
boehmite	γ-AlOOH	*Cmcm*	2.87 (2.90)	1.0	12.23 (12.04)	−1.6	3.70 (3.73)	0.8	27
gibbsite	$Al(OH)_3$	$P21/n$; $\beta = 94.54°$ (92.36°)	8.68 (8.78)	1.2	5.08 (5.10)	0.4	9.74 (9.63)	−1.1	28
akdalaite	Al_5O_8H	$P6_3mc$	5.58 (5.63)	0.9	5.58 (5.63)	0.9	8.77 (8.85)	0.9	29, 30

electron configurations were employed in the PAW potentials: $2s^22p^4$ for O, $3p^63d^74s^1$ for Fe, and $3s^23p^1$ for Al. The GGA+U method is used to correct the poor description in pure DFT/GGA of the on-site Coulomb repulsion of 3d electrons in Fe atoms. The GGA+U method modifies GGA energies with an explicit correction for the Coulomb interaction of the 3d electrons[18] and has been shown to improve experimental agreement for calculated geometries, band structures, magnetic properties,[19] and redox energies[20,21] in Fe-containing compounds. The rotationally invariant approach to the GGA+U method was used, as described by Dudarev.[22] This model approach is parametrized by a single parameter, $U_{\text{eff}} = U - J$, where U is a spherically averaged Hubbard parameter that describes the effective Coulomb interaction and J represents the screened exchange energy between electrons in the same orbital manifold. The parameters were set at $U = 4$ eV and $J = 1$ eV (or $U_{\text{eff}} = 3$ eV) for all Fe atoms unless otherwise noted, and were applied only to Fe atoms. However, to assess the optimization of the U parameter for Fe-oxyhydroxides, thermodynamic quantities were calculated over a range of U values from $U = 1$ eV (the GGA limit) to $U = 7$ eV ($U_{\text{eff}} = 0$ to 6 eV) and compared with experimentally known benchmarks. The best agreement for all materials studied is achieved for approximately $U = 4$ eV, in agreement with Rollman et al.[23]

Both hard and soft oxygen PAW potentials (calculated with energy cutoffs of 1050 and 650 eV, respectively) were tested for accuracy in multiple Fe-oxyhydroxide materials, but the results showed little dependence on the potential used when the chosen energy cutoff was sufficiently high that all output geometries and energies were converged. The electronic SCF convergence tolerance was set to 10^{-4} eV/cell, and the ionic relaxation convergence tolerance was set at 10^{-3} eV/cell for all results reported here, with the exception of calculations of vibrational frequencies. For vibrational frequency calculations, a high-precision geometry relaxation was first performed, with smaller SCF and ionic relaxation convergence tolerances of at 10^{-5} eV/cell and 10^{-4} eV/cell, respectively. The high precision relaxation is done to obtain atomic positions located more precisely at energetic minima for the subsequent calculation of vibrational frequencies. All results presented in this paper were obtained with the soft oxygen potential, which is less computationally intensive, and using an energy cutoff of 650 eV and a k-point mesh with a density per a reciprocal atom of approximately 5000 or more. A shifted Monkhorst-Pack[24] mesh is used for all structures except ferrihydrite and akdalaite, where a k-point mesh centered at the origin (Gamma) was employed, as the structure is hexagonal. Results were converged within 1−2 meV per atom with respect to energy cutoff and k-point density. All calculated data shown in this paper for hematite, goethite, and lepidocrocite result from spin-polarized calculations performed using the experimental antiferromagnetic ground states.[2] The magnetic structure for ferrihydrite is not experimentally known and has been predicted in this work. Aluminum-based structures were calculated as nonmagnetic. The predicted Fe and Al structural information is compared to experimental data in Table 2. The errors in lattice parameters are generally around 1%, which is typical for DFT GGA studies. A notable exception, where a significantly larger error is observed, is the c lattice parameter for ferrihydrite, which is discussed in detail in Section IV.A.

B. Thermodynamic Model. A primary goal of this work is to compare enthalpies and free energies predicted by DFT for Fe- (or Al-) oxyhydroxides with experimental values. These comparisons will both assess the GGA+U methods being applied here and determine the energetics implied by the Michel ferrihydrite structure. To make such comparisons possible, it is necessary to compare energetics at the same temperature, which is typically room temperature for the experimental data. As the DFT energetics are effectively at zero temperature, they are adjusted for the effects of finite temperature using experimental specific heat values; the details of this approach are given in this section. In addition, the relevant

(19) Rollmann, G.; Rohrbach, A.; Entel, P.; Hafner, J. *Phys. Rev. B* **2004**, *69*(16), 165107.
(20) Zhou, F.; Cococcioni, M.; Marianetti, C. A.; Morgan, D.; Ceder, G. *Phys. Rev. B* **2004**, *70*(23), 235121.
(21) Wang, L.; Maxisch, T.; Ceder, G. *Phys. Rev. B* **2006**, *73*(19), 195107.
(22) Dudarev, S. L.; Botton, G. A.; Savrasov, S. Y.; Szotek, Z.; Temmerman, W. M.; Sutton, A. P. *Phys. Status Solidi A* **1998**, *166*(1), 429–443.
(23) Rollmann, G.; Entel, P.; Rohrbach, A.; Hafner, J. *Phase Transitions* **2005**, *78*(1−3), 251–258.
(24) Monkhorst, H. J.; Pack, J. D. *Phys. Rev. B* **1976**, *13*(12), 5188–5192.
(25) Saalfeld, H. *Z. Kristallogr.* **1964**, *120*, 342–348.
(26) Hill, R. J. *Phys. Chem. Minerals* **1979**, *5*(2), 179–200.
(27) Corbato, C. E.; Tettenhorst, R. T.; Christoph, G. G. *Clays Clay Minerals* **1985**, *33*(1), 71–75.
(28) Saalfeld, H.; Wedde, M. *Z. Kristallogr.* **1974**, *139*(1−2), 129–135.
(29) Yamaguchi, G.; Okumiya, M.; Ono, S. *Bull. Chem. Soc. Jpn.* **1969**, *42*(8), 2247–2249.
(30) Demichelis, R.; Noel, Y.; Zicovich-Wilson, C. M.; Roetti, C.; Valenzano, L.; Dovesi, R. *J. Phys.: Conf. Ser.* **2008**, 117.

transformation reactions typically involve water, whose energy must also be calculated. Direct DFT calculation of room temperature liquid water energetics is very challenging and not the focus of the present study. Therefore, below we describe a semiempirical approach to obtain accurate water energetics with the same reference state as the DFT solid phase calculations. This section will focus on the determination of enthalpy. Although some free energy results will be given in the paper, no effort is made to calculate entropic contributions from DFT; the nonenthalpic free energy contributions are treated entirely empirically. The free energy approach is described with the free energy results in Section IV.C.

Relative stabilities will be calculated as enthalpies of reaction (or transformation) from solid hematite α-Fe_2O_3 (or for Al, corundum, α-Al_2O_3) and liquid water, and normalized to one mole of Fe atoms (or Al atoms). As an example, eq 3 shows the reaction enthalpy of goethite (FeOOH) relative to hematite. $\Delta H_{rxn}^{hem \rightarrow goe}$ refers to the enthalpy of reaction ("*rxn*") for the (hypothetical) transformation of hematite into goethite.

$$\Delta H_{rxn}^{hem \rightarrow goe} = \Delta H_f^{\mathrm{FeOOH}} - \frac{1}{2}[\Delta H_f^{\mathrm{Fe_2O_3}} + \Delta H_{\mathrm{H_2O}}^{liquid}] \quad (3)$$

The complete room-temperature enthalpy for a solid phase at temperature T is given by

$$\Delta H_f(T) = \Delta H_f^{abinitio} + \mathrm{ZPE} + \int_0^T C_p(T)\,\mathrm{d}T$$
$$= \Delta H_f(0\ \mathrm{K}) + \int_0^T C_p(T)\,\mathrm{d}T \quad (4)$$

where $\Delta H_f^{abinitio}$ is the DFT energy, ZPE is the calculated zero-point energy contribution, and $C_p(T)$ is the specific heat per Fe of the solid phase. $\Delta H_f(0\ \mathrm{K})$ is the calculated enthalpy at 0 K, which includes both the DFT energy and the ZPE. Note that no distinction is made between enthalpies and energies, as the results are for standard pressure conditions (1 atm) and the pressure contributions to the enthalpy are a fraction of a meV/atom and can be approximated as zero. While elemental reference states will affect the specific values for the enthalpies in eqs 3 and 4, the reference states cancel from the overall enthalpy of reaction in eq 3. As the reaction enthalpy is the focus of this work and only reaction enthalpies will be given the elemental reference states will not be specified or discussed. Equation 4 can also be used to obtain $\Delta H_f(0\ \mathrm{K})$ from finite temperature experimental enthalpy data, as done for the Al and Fe compounds of interest in Table 3. Table 3 can be used for direct comparison to DFT energies ($\Delta H_f^{0\mathrm{K}}$), as reported later, or alternatively to shift DFT values (by $H^{298.15\mathrm{K}} - H^{0\mathrm{K}}$) for comparison to room temperature values ($\Delta H_f^{298.15\mathrm{K}}$).

Table 3. Experimental Formation Enthalpies of Fe and Al Oxyhydroxides at Standard Conditions (298.15 K, 1 atm), Extrapolated to 0 K Using Low Temperature Specific Heat Measurements[a]

structure	$\Delta H_f^{298.15\mathrm{K}}$ (kJ/mol)	$H^{298.15\mathrm{K}} - H^{0\mathrm{K}}$ (kJ/mol)	$\Delta H_f^{0\mathrm{K}}$ (kJ/mol)
hematite	-826.2 ± 1.3[3]	15.560[31]	−841.8
goethite	-561.5 ± 1.5[3]	10.74[32]	−572.2
lepidocrocite	-552.0 ± 1.6[3]	11.05[32]	−563.1
corundum	-1675.7 ± 1.2[33]	13.58[34]	−1689.3
diaspore	-1002.7 ± 1.0[33]	6.85[35]	−1009.6
boehmite	-996.10 ± 1.30[33]	7.075[36]	−1002.95
gibbsite	-1293.1 ± 1.2[33]	12.456[37]	−1305.6

[a] Citations give the source for the formation enthalpy value or the specific heat.

ZPEs for solid Fe-oxyhydroxides are estimated for each structure assuming the only significant contribution comes from H vibrations. This approximation is justified both by the fact that the heavier Fe and O atoms will have smaller zero-point contributions than H and that the Fe and O contributions will largely cancel in the calculation of relative reaction enthalpies due to the generally similar coordination environments of these atoms in both product and reactant oxyhydroxide structures. The H ZPE is evaluated in the local harmonic approximation (all other atoms fixed), which is expected to be accurate due to the lighter mass of H compared to the other atoms.[38,39] Small displacements about the equilibrium position of the H atom, with other atoms held fixed, allow the determination of the corresponding force constant matrices, which are diagonalized to yield the vibrational frequencies and normal modes.[40] The ZPE is obtained as the sum of the contributions from each H mode, as shown in eq 5.

$$\mathrm{ZPE} \approx \frac{1}{2}\sum_i h\nu_i^{\mathrm{H}} \quad (5)$$

Here h is Planck's constant and ν_i^{H} is a vibrational frequency for an H atom. The summation runs over all $3N$ vibrational modes derived from the N H atoms in the cell. The ZPE contribution is simply added to the calculated internal energy of the system to construct the enthalpy of the structure at 0 K, as shown in eq 4. The calculated vibrational frequencies and predicted ZPE value for each compound considered in this study are given in Table 4. The calculated frequencies are largely in agreement with previous DFT studies on Al- and Fe-oxyhydroxide vibrational frequencies[41−43] and with

(31) Gronvold, F.; Westrum, E. F. *J. Am. Chem. Soc.* **1959**, *81*(8), 1780–1783.
(32) Majzlan, J.; Lang, B. E.; Stevens, R.; Navrotsky, A.; Woodfield, B. F.; Boerio-Goates, J. *Am. Mineral.* **2003**, *88*(5−6), 846–854.
(33) Robie, R. A.; Hemingway, B. S. *U.S. Geol. Surv. Bull.* **1995**, 2131.
(34) Ditmars, D. A.; Ishihara, S.; Chang, S. S.; Bernstein, G.; West, E. D. *J. Res. Natl. Bureau Stand.* **1982**, *87*(2), 159–163.
(35) Perkins, D.; Essene, E. J.; Westrum, E. F.; Wall, V. J. *Am. Mineral.* **1979**, *64*(9−10), 1080–1090.
(36) Hemingway, B. S.; Robie, R. A.; Apps, J. A. *Am. Mineral.* **1991**, *76* (3−4), 445–457.
(37) Hemingway, B. S.; Robie, R. A.; Fisher, J. R.; Wilson, W. H. *J. Res. U.S. Geol. Surv.* **1977**, *5*(6), 797–806.
(38) Jiang, D. E.; Carter, E. A. *Surf. Sci.* **2003**, *547*(1−2), 85–98.
(39) Jiang, D. E.; Carter, E. A. *Phys. Rev. B* **2004**, *70*(6), 064102.
(40) Born, M.; Huang, K. *Dynamical Theory of Crystal Lattices*; Oxford University Press: New York, 1954.
(41) Kubicki, J. D.; Paul, K. W.; Sparks, D. L. *Geochem. Trans.* **2008**, 9.
(42) Demichelis, R.; Noel, Y.; Civalleri, B.; Roetti, C.; Ferrero, M.; Dovesi, R. *J. Phys. Chem. B* **2007**, *111*(31), 9337–9346.
(43) Rosso, K. M.; Rustad, J. R. *Am. Mineral.* **2001**, *86*(3), 312–317.

Table 4. Calculated 0 K Vibrational Wavenumbers and Associated Zero-Point Energies for H Atoms in Fe- and Al-Oxyhydroxides[a]

structure	H vibrational wavenumbers (cm^{-1})	zero-point energy kJ/(mol H)
goethite	2985, 1016, 954	29.6
lepidocrocite	2789, 1069, 1012	29.1
ferrihydrite	3574, 699, 502	28.5
diaspore	2761, 1173, 1099	30.1
boehmite	2921, 1108, 1097	30.6
gibbsite		
H1	3720, 798, 715	31.9 (avg. of six H positions)
H2	3600, 880, 643	
H3	3470, 1068, 905	
H4	3531, 980, 878	
H5	3413, 1094, 902	
H6	3392, 1060, 986	

[a] The gibbsite primitive cell has six symmetry distinct H-atoms so vibrational wavenumbers are calculated for each site and the average zero-point energy is given.

experimental IR spectra.[2,44] For example, O−H stretch in goethite has been measured by Cambier at 3150 cm^{-1}, with uncoupled O−H bending modes at 850 and 938 cm^{-1}.[44] The calculated wavenumbers are all within 8% of these experimental values. Interestingly, it is found that the ZPE for the compounds of a given cation (Fe or Al) all fall within a narrow range of less than 2 kJ/(mol H) of each other, suggesting that this contribution plays a small role in relative stability overall.

In order to apply eq 3 it is necessary to determine the enthalpy of liquid water with the same reference as the DFT based solid-phase energies. Due to the unavailability of low-temperature thermodynamic data for liquid water (from near 0 K to room temperature) and the considerable difficulty of modeling bulk liquid water with DFT, the correction proposed by Wolverton et al.[45] is here extended to simplify the calculation of the enthalpy of liquid water at arbitrary temperature. In this approach DFT is used to calculate the energy of an isolated water molecule at 0 K, which is then extended to finite temperature by analytic thermodynamic expressions and then finally adjusted to give the enthalpy of liquid water by subtracting the heat of vaporization. The expression for the water enthalpy at finite temperature in our approach is given by

$$\begin{aligned}\Delta H_{H_2O}^{liquid}(T) &= E_{H_2O}^{molecule} + \Delta H_{H_2O}^{excitations}(T) - \Delta H_{H_2O}^{vaporization}(T) \\ &= E_{H_2O}^{molecule} + 16.69\text{kJ/mol} \quad \text{at} \\ T &= 298.15\text{ K} \end{aligned} \tag{6}$$

The description of the terms in this expression and the derivation of the final value on the second line are given here. $E_{H_2O}^{molecule}$ is the internal energy of the water molecule in isolation at zero temperature and is modeled by DFT calculation of a single water molecule in a periodic supercell measuring 10 × 10 × 10 Å. The size of the box is such that the calculated energy of the system is converged within about 1 meV/molecule relative to an infinite box, indicating no intermolecular interactions due to periodic boundary conditions. The DFT internal energy of the isolated molecule is then augmented by $\Delta H_{H_2O}^{excitations}(T)$, which contains the vibrational, rotational, and translational contributions to the enthalpy at finite temperature (note − this term also includes zero-point vibrational energy, which is not a thermal excitation, but still a distinct addition to the internal energy). The $\Delta H_{H_2O}^{excitations}(T)$ contributions are obtained from experimental parameters and analytic expressions as a function of temperature[46] and together with $E_{H_2O}^{molecule}$ approximate the enthalpy of steam at arbitrary temperature. The equation for the finite temperature excitation contribution to the enthalpy is[46]

$$\begin{aligned}\Delta H^{excitations}(T) = k_B \sum_{j=1}^{3} \left(\frac{\theta_{D,j}}{2} + \frac{\theta_{D,j} \cdot e^{-\theta_{D,j}/T}}{1 - e^{-\theta_{D,j}/T}} \right) \\ + \left(\frac{3}{2} k_B T\right)_{rot.} + \left(\frac{3}{2} k_B T\right)_{trans.} \end{aligned} \tag{7}$$

The first summation is over the two O−H stretching and single O−H−O bending frequencies in the water molecule, as obtained from ref 46 (Debye temperatures for these modes are θ_D = 5360, 5160, and 2290 K, respectively, where $\theta_D = h\nu/k_B$). The contributions from the rotational degrees of freedom are modeled classically. While fully quantum mechanical models for the rotational degrees of freedom have been developed, the low Einstein temperatures for H atom degrees of freedom make the classical approximation used in eq 7 very accurate above about 50 K. The excitations contribute a value $\Delta H_{H_2O}^{excitations}$ (298.15 K) = 60.70 kJ/mol at room temperature (the bulk of this contribution comes from the ZPE of the water). Finally, the enthalpy of vaporization of liquid water to steam, $\Delta H_{H_2O}^{vaporization}$, is subtracted from the total energy of the H_2O model to obtain the enthalpy of liquid water. The enthalpy of vaporization of water at room temperature is $\Delta H_{H_2O}^{vaporization}$ (298.15 K) = 44.01 kJ/mol.[47] Combining the values for $\Delta H_{H_2O}^{excitations}$ (298.15 K) and $\Delta H_{H_2O}^{vaporization}$ (298.15 K) yields the second line in eq 6.

By combining eq 4 and eq 5 for the solid phases and eq 6 and eq 7 for liquid water, we can now apply eq 3 to predict DFT-based finite temperatures reaction energetics for the Fe- and Al-oxyhydroxides. In order to assess the accuracy of the overall approach, and, in particular, our expression for $\Delta H_{H_2O}^{liquid}(T)$ in eq 6, we have applied eq 3 to predict the enthalpies of transformation of Al-oxyhydroxide phases and compared them to experimental data. The Al-oxyhydroxides are a logical set of test compounds to assess our approach, given that they are isostructural to the Fe-oxyhydroxides (with the exception of gibbsite, which has no confirmed Fe-based isostructure).

(44) Cambier, P. *Clay Minerals* **1986**, *21*(2), 191–200.
(45) Wolverton, C.; Hass, K. C. *Phys. Rev. B* **2000**, *63*(2), 024102.
(46) McQuarrie, D. A.; Simon, J. D. *Molecular Thermodynamics*; University Science Books: Sausalito, CA, 1999.
(47) Atkins, P. *Physical Chemistry*, 6th ed.; W.H. Freeman and Co.: New York, 1997.

Table 5. Experimental, Uncorrected Calculated, and Corrected Calculated Relative Stabilities at 298.15 K, 1 atm for the Al-Oxyhydroxides Relative to Corundum, α-Al_2O_3 + water

Structure	ΔH_{rxn}^{expt} (experiment) kJ/(mol-Al)	$\Delta H_{rxn}^{abinitio}$ (uncorrected) kJ/(mol-Al)	$\Delta H_{\mathrm{rxn}}^{abinitio}$ (corrected via eq 6) kJ/(mol-Al)
diaspore, α-AlOOH	-20.55 ± 2.6[33]	−9.6	−17.9
boehmite, γ-AlOOH	-15.65 ± 2.6[33]	−13.3	−21.6
gibbsite, $Al(OH)_3$	-26.55 ± 1.8[33]	0.4	−24.6

Table 5 shows the calculated stabilities (enthalpies of reaction) for diaspore, boehmite, and gibbsite relative to corundum and water. The uncorrected energies use only the DFT energy for the isolated water molecule, that is, $\Delta H_{\mathrm{H_2O}}^{liquid}(T) = E_{\mathrm{H_2O}}^{molecule}$. The corrected energies, meanwhile, use the full expression for $\Delta H_{\mathrm{H_2O}}^{liquid}(T)$ presented in eq 6. Note that the large errors relative to experiment for the uncorrected energies are greatly reduced by including the water corrections, demonstrating their importance and their (at least qualitative) accuracy.

The final, predicted reaction enthalpies for Al-oxyhydroxides remain in somewhat poor agreement with experiment, with errors of up to 6 kJ/(mol-Al) in size. However, this is almost certainly not attributable to an error in $\Delta H_{\mathrm{H_2O}}^{liquid}(T)$, as there is no consistent trend toward under- or overestimation of the errors. To show that the Al-oxyhydroxide calculated energies are, on average, consistent with our water model, we can fit the non-DFT terms in eq 6 and compare the result to our model. First we write

$$\Delta H_{\mathrm{H_2O}}^{liquid}(T) = E_{\mathrm{H_2O}}^{molecule} + \Delta H_{\mathrm{H_2O}}^{excitations}(T) - \Delta H_{\mathrm{H_2O}}^{vaporization}(T) = E_{\mathrm{H_2O}}^{molecule} + \delta h_{corr} \quad (8)$$

where δh_{corr} contains all the corrections necessary to correct the molecular DFT water energy so as to better match experimental physical conditions. Now, if rather than using experimental values for the terms in δh_{corr}, it is instead fit to minimize the least-squares error in the predicted vs experimental reaction enthalpies in Table 5 then one obtains $\delta h_{corr} = 14.9$ kJ/mol. This is quite close to the value of 16.7 kJ/mol obtained analytically for the second two terms in eq 6, in support of the assertion that these terms yield an accurate representation of the energetics, and that the DFT based water energy is close to experiment. The discrepancies between predicted and measured enthalpies in the Al-oxyhydroxides are therefore likely due to errors in the experimental determinations, or in the DFT solid phase energetics. Section IV.C discusses the application of this thermodynamic model to the Fe-oxyhydroxides.

IV. Results

Section IV describes the results of detailed DFT-based modeling of ferrihydrite in the Michel structure. Section IV.A focuses on the optimized geometry, where the primary goal is to determine whether the DFT-derived atomic positions are consistent with those given in the Michel model. Such agreement is neither trivial to demonstrate nor a foregone conclusion, as the DFT based model proceeds from conjectured initial H positions, predicts a new magnetic structure, removes all partial occupancies, and, moreover, corresponds to a idealized bulk phase, in contrast to the nanoparticulate form characterized experimentally. Section IV.B presents and discusses the results obtained from the magnetic modeling, and compares such with the limited experimental results on magnetic structure. The magnetic study is of interest in its own right, but also essential for providing the correct magnetic arrangement for the structural studies in IV.A and the energetic studies in IV.C. Finally, Section IV.C provides a validation of the GGA+U approach used in all of the foregoing sections, and evaluates the energy and relative stability of ferrihydrite in the Michel structure.

A. Ferrihydrite Bulk Structure. GGA+U calculations, adopting the predicted groundstate ferrimagnetic ordering model (see Section IV.B on magnetic model for ferrihydrite), yield the structural data for bulk crystalline ferrihydrite shown in Table 6. Calculated geometries largely agree with those given by Michel et al. The H positions were not determined in the original experimental study[1] and so approximate initial H positions have been taken from DFT structural optimizations of the isostructural Al-based material akdalaite.[30] The H positions were then fully relaxed in the ferrihydrite structure. Figure 1 shows the calculated bonding geometries of the three symmetry-distinct Fe polyhedra, and the equilibrium H positions. Table 7 presents the calculated relaxed fractional coordinates of all symmetry-distinct atoms in the ferrihydrite unit cell.

The most notable discrepancy between the experimental and the DFT calculated geometries (Table 6) is the considerable overestimation of the *c*-lattice parameter compared to the Michel et al. data, the GGA+U value exceeding that reported for 6-line ferrihydrite by 2.4%. However, it is clear from Table 6 that the *c*-lattice parameter is sample dependent, and evidently increases from 2-line to 6-line ferrihydrite. The appearance of more lines in the diffraction pattern typically corresponds to larger particles with higher crystallinity. In addition, the refinements reported by Michel et al. suggest that the larger particles have significantly fewer cation vacancies, tending toward full occupation of all Fe sites for more highly crystalline samples. Taken together, these observations suggest a trend toward increasing c-lattice parameter with increasing particle size (and associated increased crystallinity and reduced vacancy content). Recent results on even larger particles of highly crystalline ferrihydrites from Michel suggest that the *c* lattice parameter continues to expand,[48] and that crystalline ferrihydrite would have a *c* lattice constant of 9.36(3) Å, quite

(48) Michel, F. M.; Cismasu, C.; Strongin, D. R.; Parise, J. B.; Brown, G. E., Jr. Real-space structural analysis of ferrihydrite nanoparticles. Presented at The 237th ACS National Meeting, Salt Lake City, UT, March 24, 2009.

Table 6. Comparison of Calculated and Experimental Lattice Parameters and Selected Calculated Bond Lengths and Angles for Ferrihydrite[a]

	GGA+U (U = 4 eV) (bulk crystalline)	expt. Michel et al.[1] (in order of most to least crystalline)		
		6-line	3-line	2-line
space group	$P6_3mc$	$P6_3mc$	$P6_3mc$	$P6_3mc$
a (Å)	5.97	5.9289	5.9537	5.9587
c (Å)	9.37	9.1267	9.0967	8.9657
volume (Å^3)	289.6	277.8	279.2	275.7
O−H (Å)	1.00			
H Bond (Å)	2.35			
Fe1−O_{oct} (Å)	1.981(×2), 2.040, 2.068, 2.075(×2)	1.933, 2.012(×2), 2.140(×2), 2.042	1.923, 2.005, 2.017, 2.140(×2), 2.064	1.918, 1.979(×2), 2.036(×2), 2.052
Fe2−O_{oct} (Å)	1.952(×3), 2.206(×3)	1.874(×3), 1.964(×3)	1.879(×3), 1.985(×3)	1.883(×3), 2.082(×3)
Fe3−O_{tet} (Å)	1.916(×1) 1.923(×3)	1.790(×1) 1.953(×3)	1.773(×1) 1.961(×3)	1.959(×1) 2.019(×3)
Fe−O−H (deg)	123			
O−H···O (deg)	133			

[a] The notation ×N denotes N bonds of the same length. Note the increase in the c-lattice parameter and cell volume with increasing crystallinity.

Table 7. DFT Irreducible Atom Coordinates for Ferrihydrite (fractional coordinates, relaxed from Michel geometry[1])[a]

atom (spin)	a	b	C
Fe1 (up)	0.1668	0.8332	0.6336
Fe2 (down)	0.3333	0.6667	0.3353
Fe3 (down)	0.3333	0.6667	0.9545
O1	0.0000	0.0000	0.0124
O2	0.3333	0.6667	0.7501
O3	0.1672	0.8328	0.2368
O4	0.5145	0.4855	0.0000
H1	0.0000	0.0000	0.4062

[a] Spin states (up/down) used for Fe sites in the calculation are given and described in detail in Section IV.B.

Table 8. Experimental Low-Temperature Magnetic Structures and Magnetic Transition Temperatures of the Fe-Oxides and Oxyhydroxides[2,50−55]

structure	experimental magnetic ordering at 0 K	magnetic transition temperature (K)
hematite	antiferromagnetic	260 (Morin transition)[2]
		948 (Néel transition)[2]
goethite	antiferromagnetic	400 (Néel transition)[2]
lepidocrocite	antiferromagnetic	77 (Néel transition)[2]
magnetite	ferrimagnetic	120 (Verwey transition)[2]
		850 (Curie transition)[2]
maghemite	ferrimagnetic	820−986 (Curie transition)[2]
ferrihydrite	AFM /ferrimagnetic	120−550 (Néel transition)[50−55]
		250 (Néel transition—this work)

Table 9. Calculated Energy Differences Separating Ferromagnetic (FM) and Groundstate (GS) Orderings in Fe-Oxyhydroxides

structure	FM-GS energy, kJ/(mol-Fe)
hematite	+25.7
goethite	+15.4
lepidocrocite	+3.3
ferrihydrite	+20.0

similar to our predicted value.[49] Therefore, we believe that our structural predictions, which describe ideal crystalline bulk ferrihydrite with no vacancies, constitute an accurate representation of the bulk, undefected Michel model structure.

The ferrihydrite bulk crystal structure obtained here may also help to resolve a concern about the tetrahedral Fe3 positions arising in the Michel model. The asymmetry and bond lengths of this site were identified as problematic in a recent criticism of the Michel model by Manceau:[6] the experimental tetrahedral Fe−O bond distance along the c-axis of the structure is only 1.790 Å, while the 3 other Fe−O bonds in the tetrahedron are 1.952 Å in length. The bond-length of 1.790 Å is considerably shorter than would be expected for tetrahedral Fe^{III}. However, the bulk crystalline DFT-relaxed structure of ferrihydrite obtained here shows an approximately symmetrical tetrahedral Fe3−O bonding arrangement, with 4 Fe−O bonds of nearly equivalent length (1.916 Å × 1, 1.923 Å × 3) consistent with tetrahedral Fe^{III}. Careful examination of the experimental and calculated structures shows that the c lattice parameter discrepancy described above is due to the variations in Fe3−O bond distances between the experimental and calculated geometries. Therefore, the calculations suggest that the unusual Fe3−O bond length is not inherently part of the undefected Michel structure, but instead may be a byproduct of surface effects, poor crystallinity, defects, and/or refinement errors on small nanoparticles. More specifically, the Michel model cannot be interpreted as implying that Fe3 sites in a putative bulk crystalline phase would manifest one short Fe3−O bond of length 1.79 Å.

B. Modeling Magnetism in Ferrihydrite. To accurately model thermodynamic properties of Fe-oxide and oxyhydroxide materials, close attention must be paid to the specific arrangement of the magnetic moments borne by Fe atoms in the crystal lattice. The energies associated with changes in the magnetic ordering in Fe-oxyhydroxides are often of larger magnitude than the differences in the relative stabilities of the structures. Hematite, goethite, and lepidocrocite are all antiferromagnetic at low temperatures, with specific spin arrangements and magnetic ordering temperatures as presented in Table 8.[2] For these materials, failure to model the correct magnetic orderings causes significant errors in calculated energies. Table 9 presents the DFT-derived energy differences separating the hypothetical ferromagnetic ordering from the magnetic ground state. The experimentally determined antiferromagnetic ground states are applied in all cases, save for ferrihydrite, where the ground state ordering is ferrimagnetic, as obtained in the present work. Note

(49) Michel, F. M. Personal communication, **2009**.

Table 10. Selected Experimental Studies of Magnetism in Ferrihydrite

study	T_N (K), Néel temperature	low-temperature ordering	method(s)
Pankhurst et al. (1992)[53]	n/a	2-line: ferrimagnetic 6-line: antiferromagnetic	low-temperature Mössbauer spectroscopy
Zergenyi et al. (2000)[50]	120	antiferromagnetic with parasitic ferromagnetic moment	Mössbauer spectroscopy, magnetometry
Seehra et al. (2000)[55]	350	antiferromagnetic with uncompensated surface spins	neutron scattering
Guyodo et al. (2006)[51]	500−550	antiferromagnetic with ferromagnetic-like moment due to uncompensated spins	Mössbauer spectroscopy, magnetometry
Berquó et al. (2007),[56] Berquó et al. (2009)[57]	422	antiferromagnetic, superparamagnetic interactions likely increase for small, agglomerated particles	Mössbauer spectroscopy, magnetometry, HRTEM, XRD

that we are interested here in obtaining only the zero-temperature magnetic energetics for the solid phases, for the effects of the finite-temperature magnetism upon the thermodynamic quantities (e.g., the Néel transition in lepidocrocite and the Morin transition in hematite) are all included through the integration of experimental specific heats (see eq 4).

The low temperature magnetic properties of bulk ferrihydrite are not well-known, as experimental studies of the magnetic properties of ferrihydrite are complicated by uncertainties in particle size, structure, and surface effects. In addition, ferrihydrite particles are often agglomerated into clusters where interparticle magnetic interactions are expected. Superparamagnetism, in which the net ferromagnetic moments of nanoparticles are subject to flipping due to thermal fluctuations, is observed in nanoparticle samples at temperatures greater than 120 K.[50] Superparamagnetic and particle-size dependent magnetic effects have been confirmed and further resolved in investigations on ferrihydrite particles coated with sugar or alginate to reduce or eliminate interparticle interactions.[56,57] Previous studies[50−55] suggest a ferrimagnetic or antiferromagnetic ordering for ferrihydrite at low temperature, where, in the case of antiferromagnetism, the presence of remnant ferromagnetic moments associated with uncompensated spins randomly distributed in either the bulk or at the surface of the nanoparticles is often suggested. Experimental estimates of the Néel ordering transition temperature in ferrihydrite range from 120 K to over 500 K (see Table 10). Comparison of the neutron scattering- and X-ray diffraction data suggests that the magnetic and crystallographic unit cells are equivalent.[55] However, absent a fully descriptive crystallographic structural model, previous studies have not determined a specific magnetic ordering arrangement for ferrihydrite.

This study investigates the magnetic ordering arrangement of bulk crystalline ferrihydrite using a pairwise magnetic interaction model (Heisenberg model) developed for the ferrihydrite structure. The approach follows that used by Morgan et al.,[58] wherein the Heisenberg model parameters were fitted to reproduce the DFT energies of different magnetic orderings. The set of magnetic structures for fitting was initially taken to include all the symmetry-distinct collinear antiferromagnetic arrangements representable in the primitive Michel model unit cell, based on the assumption that an antiferromagnetic ground state would prevail. Using the Alloy Theoretic Automated Toolkit (ATAT) code,[59] a set of 36 symmetry-distinct antiferromagnetic arrangements were identified, each containing 10 Fe atoms (arranged 5 spin−up and 5 spin−down). An attempt was made to obtain energies for all of these magnetic states, but convergence problems resulted for approximately half of them, likely due to initialization in a highly unstable magnetic configuration. In the end, 19 antiferromagnetic energies and the single ferromagnetic energy were computed (including full relaxation of each structure), which together were sufficient to parametrize the Heisenberg model. Calculated magnetic moments were all high-spin and gave a value of about 4 μ_B per Fe. All pairwise (two-spin) interactions between Fe sites less than 5 Å apart were fit with the ATAT code using the 20 DFT energies. Multispin interactions (e.g., interactions between three Fe sites) were also considered, but upon fitting were found to be energetically insignificant compared to the dominant pairwise interactions. Eight pairwise interactions were used in the final fit, yielding an optimized cross-validation score of 1.2 meV/spin (amounting to 0.6% of the total 208 meV/spin range of the magnetic energies, or 2.7% of the standard deviation of the distribution of magnetic ordering energies, σ = 43.7 meV/spin). The small cross-validation score suggests that the fitted interactions represent the DFT energetics accurately.

(50) Zergenyi, R. S.; Hirt, A. M.; Zimmermann, S.; Dobson, J. P.; Lowrie, W. *J. Geophys. Res.* **2000**, *105*(B4), 8297–8303.
(51) Guyodo, Y.; Banerjee, S. K.; Penn, R. L.; Burleson, D.; Berquo, T. S.; Seda, T.; Solheid, P. *Phys. Earth Planet. Inter.* **2006**, *154* (3−4), 222–233.
(52) Silva, N. J. O.; Amaral, V. S.; Carlos, L. D. *Phys. Rev. B* **2008**, *77*, 134426.
(53) Pankhurst, Q. A.; Pollard, R. J. *Clays Clay Minerals* **1992**, *40*(3), 268–272.
(54) Punnoose, A.; Phanthavady, T.; Seehra, M. S.; Shah, N.; Huffman, G. P. *Phys. Rev. B* **2004**, *69*(5), 054425.
(55) Seehra, M. S.; Babu, V. S.; Manivannan, A.; Lynn, J. W. *Phys. Rev. B* **2000**, *61*(5), 3513–3518.
(56) Berquó, T. S.; Imbernon, R. A. L.; Blot, A.; Franco, D. R.; Toledo, M. C. M.; Partiti, C. S. M. *Phys. Chem. Minerals* **2007**, *34*(5), 287–294.
(57) Berquó, T. S.; Erbs, J. J.; Lindquist, A.; Penn, R. L.; Banerjee, S. K. *J. Phys.: Condens. Matter* **2009**, *21*(17), 176005.
(58) Morgan, D.; Wang, B.; Ceder, G.; van de Walle, A. *Phys. Rev. B* **2003**, *67*(13), 176005.
(59) van de Walle, A.; Asta, M.; Ceder, G. *CALPHAD: Comput. Coupling Phase Diagrams Thermochem.* **2002**, *26*(4), 539–553.

Table 11. Pairwise Effective Cluster Interactions (ECIs) in Ferrihydrite Primitive Unit Cell[a]

cluster number	ECI (meV/pair)	ECI (K/pair)	distance (Å)	Fe sites involved, anion sharing geometry	cluster multiplicity (per unit cell)	Fe−O−Fe angle (deg)
1	5.8	7.7	2.99	Fe1−Fe1, edge	12	92, 94
2	4.9	6.5	3.28	Fe1−Fe2, edge	6	100, 100
3	25.0	33.2	3.43	Fe1−Fe3, corner	12	118
4	31.9	42.3	3.47	Fe1−Fe3, corner	6	122
5	20.5	27.2	3.63	Fe2−Fe3, no sharing	2	
6	43.2	57.3	3.54	Fe2−Fe1, corner	12	128
7	20.5	27.2	3.63	Fe2−Fe3, corner	6	123
8	5.8	7.7	4.99	Fe1−Fe1, no sharing	12	

[a] The fifth column indicates the Fe sites involved in the pair and also the oxygen anion sharing arrangement. ECI(K/pair) defined as [ECI(*energy*)]/[$k_B S(S+1)$] with $S = 5/2$ for Fe^{III}.

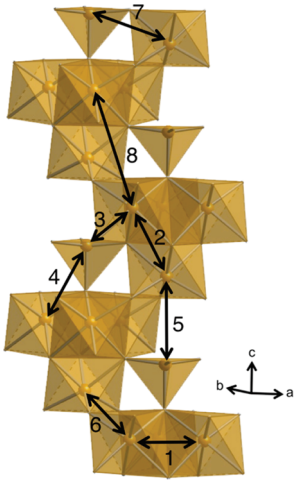

Figure 2. Pairwise spin interactions included in the Heisenberg mode for ferrihydrite. Only Fe atoms are shown for clarity.

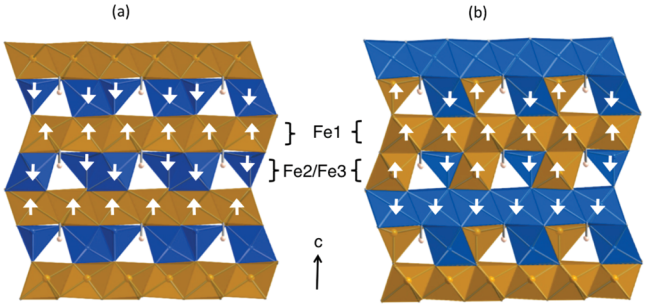

Figure 3. (a) Predicted stable ferrimagnetic ordering for ferrihydrite. O atoms are omitted for clarity. Up spins (color: brown) (greyscale: light gray) outnumber down spins (color: blue) (greyscale: dark gray) 3:2. (b) The most stable predicted antiferromagnetic ordering has energy 1 kJ/(mole-Fe) relative to ferrimagnetic groundstate ordering.

Table 11 describes the eight parametrized interactions, including the interaction distance, the Fe-sites involved, the anion sharing geometry (edge, corner, etc), the Fe−O−Fe angle subtended by the interaction, and the cluster multiplicity per unit cell. The pairs are also shown in Figure 2. The majority of the parametrized interactions proceed through one or a pair of intervening O anions, so that they are of the superexchange type. Clusters 5 and 8, however, stand as exceptions, where the coupling presumably proceeds by direct Fe−Fe overlap (more likely for cluster 5) and/or by higher order through-bond interactions such as supersuperexchange (more likely for cluster 8). The largest pairwise interaction energies are obtained for interlayer antiferromagnetic superexchange interactions (Fe1/Fe3 and Fe1/Fe2 pairs: clusters 3, 4, and 6).

Using the fitted interactions, a Monte Carlo simulation of the classical Heisenberg model was performed so as to determine the ground state magnetic ordering at low temperature. Beginning with a large supercell based on the ferrihydrite unit cell (600 ferrihydrite unit cells, length approximately 50 Å per side) with a random spin ordering at high temperature (800 K), a cooling simulation was performed in which the spins were annealed into their low-temperature ordering. A large supercell is chosen to ensure that ordered configurations were not forced by any limited dimension of the unit cell. Various supercell sizes were also tested, and it was ensured that supercell dimension had no effect upon either the ground state magnetic ordering obtained, or the transition temperature. The Monte Carlo simulation shows a transition from randomly ordered paramagnetism to ordered ferrimagnetism at 250 ± 5 K. Here, the error represents only that due to the numerical accuracy of the determination of the Néel temperature, and does not reflect the considerably larger uncertainties inherent to the model. Essentially
no hysteresis in the magnetic transition temperature was observed when the simulation is performed in reverse (heating a fully ordered cell from 0 K to high temperature), suggesting a second-order or weakly first-order transition.

The Monte Carlo simulation predicts a ferrimagnetic groundstate, as shown in Figure 3, wherein uncompensated Fe moments are distributed regularly in layers throughout the bulk (20% of moments, or two moments per unit cell, are uncompensated) (Figure 3a). Surprisingly, the low-temperature spin-alignment from the Monte Carlo simulations is slightly noncollinear. However, it is identical to a perfectly collinear ferrimagnetic state except for small, seemingly random deviations from collinearity of typically just a few degrees (never more than 10°).

The small deviation from collinearity observed in the Monte Carlo simulation is potentially a real property of the ground state, but may easily be an artifact of the Heisenberg model due to, for example, the lack of longer-range pairwise interaction energies. Removing these small noncollinear deviations, a collinear structure

corresponding to the Monte Carlo groundstate was obtained, the energy of which was further assessed within a full collinear DFT calculation. The noncollinear structure should not be misconstrued as a failure to achieve convergence of the Monte Carlo simulation, as it is actually lower in energy than the corresponding collinear structure. However, regardless of its source, the noncollinearity is of almost no energetic consequence, leading to reductions in energy of only 0.1 kJ/(mol-Fe) as compared with the corresponding collinear ferrimagnetic state when evaluated within the Heisenberg model. Thus, it is concluded that the collinear structure is a good representation of the ferrihydrite magnetic ground state. The collinear ferrimagnetic structure is used in all the ferrihydrite calculations presented in other sections of this paper and the magnetic structure is discussed in more detail below.

The predicted ferrimagnetic ground state corresponds to a layered structure in which planes of Fe moments alternate in alignment along the *c*-axis (Figure 3a). Planes of octahedrally coordinated Fe atoms (site Fe1 in the Michel model, see Figure 1) that share two O atoms along an octahedral edge show ferromagnetic ordering, indicating frustration on the spin−lattice, as all the fitted interactions favor antiferromagnetic coupling. Stronger antiferromagnetic interactions between pairs of Fe1/Fe2 and Fe1/Fe3 atoms (cluster nos. 3, 4, and 6 in Table 11) override the weaker antiferromagnetic interaction between Fe1 atoms (cluster no. 1) and put the Fe1-site spins into a ferromagnetic (like-spin) arrangement with respect to each other. The next plane of atoms along the c-direction includes the symmetry-inequivalent octahedral site (Fe2, Figure 1), and also a tetrahedral Fe site (Fe3, Figure 1), in equal proportion. The second octahedral site (Fe2) shares three corner oxygen atoms with the layer of Fe1 sites below, and three edges with the Fe1 octahedra above. The tetrahedral Fe3 site shares corner oxygen atoms with both Fe1 and Fe2 polyhedra. Antiferromagnetic ordering is found between the Fe1 and Fe2/Fe3 layers in the ferrimagnetic model. As Fe1 sites outnumber the Fe2 and Fe3 sites (six Fe1, and two each of Fe2 and Fe3 per primitive unit cell), the overall ratio of up to down moments is 3 to 2, leaving 20% of the moments uncompensated. Notably, the predicted ferrimagnetic ordering of ferrihydrite is similar to that of the ferrimagnets magnetite and maghemite, both of which also share structural elements with ferrihydrite, including mixed tetrahedral and octahedral Fe sites arranged in layers. In magnetite and maghemite, parallel spins occupy all symmetry-equivalent sites, as in the predicted ferrimagnetic ordering for ferrihydrite; antiferromagnetic ordering is observed only between symmetry-distinct sites (e.g., octahedral A sites are antiparallel to tetrahedral B sites, using the conventional site labeling scheme for magnetite and maghemite).[2]

Another Monte Carlo simulation was performed with the constraint of zero net spin, forcing an antiferromagnetic ordering to result at low temperature. The predicted low-temperature antiferromagnetic ordering is shown in Figure 3b, and also shows layering of spins stacked along the *c*-axis. The energy of this ordering was also assessed with a full collinear DFT calculation, and was found to be unstable relative to the collinear ferrimagnetic structure by slightly more than 1 kJ/(mol-Fe). Therefore, the most stable magnetic structure is the ferrimagnetic ordering, although this is nearly degenerate with a similar antiferromagnetic ordering. The antiferromagnetic stacking sequence includes ferromagnetic ordering along the planes of Fe1 sites, as in the ferrimagnetic model, albeit with alternating spin directions from layer to layer. Unlike the ferrimagnetic model, Fe2 and Fe3 sites have antiparallel spins within the same layer, and ferromagnetic ordering is observed for the Fe1−Fe2 pair identified by cluster no. 2 in Figure 2.

Proceeding on the basis that 20% of the Fe moments are uncompensated in the ferrimagnetic model, and based on the cation density of ferrihydrite (~35 Fe^{III}/nm^3), it can be shown that a 4 nm diameter spherical nanoparticle of ferrihydrite would contain roughly 230 uncompensated Fe moments, distributed regularly throughout the bulk. In the case of Fe^{III}, for which $S = 5/2$, the spin-only magnetic moment per Fe is $\mu_{Fe} = g(S(S + 1))^{1/2} \mu_B = 5.9 \mu_B$. Hence, the net magnetic moment due to uncompensated Fe moments in a 4 nm perfectly ordered ferrimagnetic particle amounts to approximately $1360 \mu_B$. This value is considerably larger than estimates based on indirect evidence in experimental studies that assume a random distribution of uncompensated spins either in the bulk, or on or near the nanoparticle surface, in which a net magnetic moment of $242-290 \mu_B$/particle is obtained (Seehra et al.[55]) Much of this difference could be explained by the high fraction of spin-bearing sites in a 4 nm particle that are impacted by defects and surfaces and therefore could deviate from the ideal ferrimagnetic ordering. Roughly 40% of all Fe atoms in a 4 nm particle can be considered "surface spins", as they are in the outer monolayer of Fe-polyhedra and have at least one missing magnetic interaction (i.e., a missing 'magnetic bond'). In addition, if even a modest fraction of Fe lattice sites within the "bulk" are vacant, local magnetic disorder due to the concomitant missing exchange interactions could noticeably affect the bulk magnetic ordering, likely reducing the net moment of a nanoparticle in the case of randomly disordered spins, and potentially affect spin ordering to the extent that a different low energy magnetic structure is stabilized. While a rigorous quantitative comparison cannot be made between the model and experimental moments at this point, the fact that a larger magnetic moment is predicted for the ideal ferrimagnetic structure than that measured for ferrihydrite nanoparticles is to be expected.

C. Fe-Oxyhydroxide Stability and GGA+U Method. To accurately model the thermodynamic properties of Fe-containing materials it is necessary to have accurate DFT energetics. In the Fe-based oxyhydroxides, the correlations between the 3d electrons localized on the same Fe atoms are not treated accurately within the GGA. The GGA+U method is employed here to correct these known errors (for specific details, see Section III.A). In previous

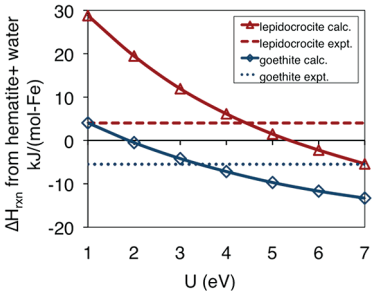

Figure 4. Calculated enthalpy for formation from hematite (and water) at 298.15 K of goethite and lepidocrocite versus the U parameter and as compared with experiment.[4] The region of best agreement with experimental thermodynamic data is achieved for $U \approx 4$ eV. For $U = 4$ eV, DFT values differ from experimental data by less than ±2.2 kJ/(mol-Fe) for both goethite and lepidocrocite.

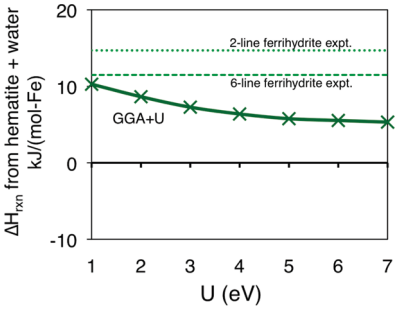

Figure 5. Calculated enthalpy of formation of bulk ferrihydrite, relative to hematite and water at 298.15 K, as a function of the U parameter. The experimental formation enthalpies of 6-line and 2-line ferrihydrite are obtained from Majzlan et al.[5] and represent samples of synthetic nanoparticles.

studies, the best agreement with experimental thermodynamic, structural, electronic, and magnetic behavior[60] in Fe-oxides was achieved at $U = 4-5.5$ eV[19,21,60−62] (or $U_{\text{eff}} = U - J = 3-4.5$ eV, with J set at a constant 1 eV, following the example of Rollman et al.[23]).

To assess the effectiveness of GGA+U for the specific set of Fe-oxyhydroxides under consideration, the energetics and relative stability of each structure have been calculated as a function of U and compared with experiment. Relative stabilities for the Fe-oxyhydroxide structures with reference to hematite and water were calculated following the methods described in Section III.B. The stabilities are calculated for a range of U values from 1 to 7 eV, or equivalently $U_{\text{eff}} = 0-6$ eV, where, again, J is fixed at 1 eV. Note that $U = 1$ is therefore equivalent to standard GGA. A significant dependence on U is observed for the relative stabilities of goethite and lepidocrocite (Figure 4). The best agreement with experimental relative thermodynamic stabilities (reaction enthalpies) is achieved for $U \approx 4$ eV, consistent with the range of optimal U values discussed above.

In a manner similar to lepidocrocite and goethite, the relative stability of bulk ferrihydrite was also obtained as a function of U, applying the ground state ferrimagnetic ordering described in Section IV.B. Low-temperature specific heat data for ferrihydrite was not available but is needed to apply the thermodynamic model described by eq 4. As an estimate of the low-temperature specific heat profile for ferrihydrite between 0 and 298.15 K, the $\int_0^{T=298.15\text{K}} C_p \, dT$ value (equivalent to $H^{298.15\text{K}} - H^{0\text{K}}$) for ferrihydrite was estimated using a linear combination of the values for hematite and goethite ($\int_0^{T=298.15\text{K}} C_p dT =$ 15.56 and 10.74 kJ/(mol-Fe), respectively), based on the fact that the ferrihydrite stoichiometry can be formed from two parts hematite and one part goethite formula units (eq 9), and the observation that, as a first approximation, formation enthalpy is mainly dependent on stoichiometry (or in the case of Fe-oxides and oxyhydroxides, degree of hydration). The proxy materials used to predict the ferrihydrite specific heat (hematite and goethite) do not have a magnetic disordering transition between 0 and 298.15 K. To account for the presence of this transition in ferrihydrite an additional term is added to the ferrihydrite enthalpy. This term is determined from the Monte Carlo simulation of the ferrihydrite magnetic Heisenberg model described in Section IV.B. The enthalpy as a function of temperature shows a smooth increase until near $T_N \approx 250$ K, at which point it jumps significantly. The difference between the extrapolated enthalpy based on the low temperature behavior and the actual enthalpy at 298.15 K is 0.7 kJ/(mol-Fe), which is taken to be the enthalpy associated with the magnetic disordering transition. This term has therefore been added to the enthalpy determined from the proxy materials to account for the magnetic disordering and is included in eq 10.

$$2 \cdot Fe_2O_3 + FeOOH \rightarrow Fe_5O_8H \tag{9}$$

Normalizing per mole of Fe atoms, the $\int_0^{T=298.15\text{K}} C_p \, dT$ value for ferrihydrite is estimated as

$$\int_0^{T=298.15\text{K}} C_p \, dT_{ferrihydrite} = \frac{2}{5}(15.56) + \frac{1}{5}(10.74) + 0.7 = 9.07 \text{ kJ/(mol-Fe)} \tag{10}$$

All of the Fe-oxyhydroxides studied in this paper display similar low-temperature specific heat profiles, with $\int_0^{T=298.15\text{K}} C_p \, dT$ values ranging from 7.78 to 10.83 kJ/(mol-Fe), so basing our estimated thermodynamic correction for ferrihydrite upon the data for other structures besides hematite and goethite would likely yield a shift of only 1−2 kJ/(mol-Fe), at most, in the calculated relative stability of ferrihydrite. At $U = 4$ eV, bulk crystalline ferrihydrite is predicted to be metastable in terms of formation enthalpy relative to hematite + water, as can be seen in Figure 5. At 298.15 K, the standard formation enthalpy of ferrihydrite is calculated as $\Delta H°_f$ (Fe_5O_8H) = −435.3 kJ/(mol-Fe) relative to the elements

(60) Bengtson, A.; Persson, K.; Morgan, D. *Earth Planet. Sci. Lett.* **2008**, *265*(3−4), 535–545.
(61) Tsuchiya, T.; Wentzcovitch, R. M.; da Silva, C. R. S.; de Gironcoli, S. *Phys. Rev. Lett.* **2006**, *96*(19), 198501.
(62) Lee, Y.-L.; Morgan, D. *Phys. Rev. B* **2009**, accepted for publication.

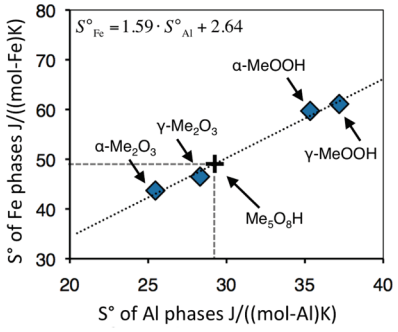

Figure 6. Linear correlation of the standard entropies of isostructural Fe- and Al-oxyhydroxides (following the approach of Majzlan et al.[5]). The standard entropy of ferrihydrite is estimated to be 49.1 J/(mol-Fe K) based on the correlation of known entropy values and assuming ferrihydrite Fe_5O_8H corresponds to the aluminum isostructure akdalaite, Al_5O_8H (marked with a "+"). Error bars for experimental standard entropies are smaller than the symbol size (less than 0.5 J/(mol-Me K)).

Table 12. Gibbs Free Energies of Formation Relative to Hematite + Water for the Fe-Oxyhydroxides at $T = 298.15$ K and 100% Relative Humidity[a]

structure	$\Delta G_{rxn}^{experiment}$, kJ/(mol-Fe)	ΔG_{rxn}^{GGA+U} kJ/(mol-Fe)
hematite	0.00	0.00
goethite	0.15[3]	−1.5
lepidocrocite	8.05[3]	10.2
ferrihydrite (bulk)	n/a	6.9

[a] Calculated results shown for $U = 4$ eV.

in their standard states or 6.4 kJ/(mol-Fe) relative to hematite + liquid water. The significant deviation (5−9 kJ/(mol-Fe)) from the experimental enthalpies (Figure 5) is interpreted as being due to particle size effects and will be discussed in Section IV.D.

Next, the enthalpy calculation is extended to give an estimate for the Gibbs energy of bulk ferrihydrite, which is a better gauge of overall stability. To evaluate this quantity is it necessary to determine the standard entropy $S°$ (as standard free energy, $G° = H° - TS°$). We estimated the standard entropy of the bulk ferrihydrite phase following the method of Majzlan et al.[5] in which an empirical relationship is fitted to interpolate between the entropies of isostructural Fe^{III} and Al^{III}-based oxyhydroxides whose standard entropy values are known (Figure 6). The Majzlan study estimated the standard entropy of ferrihydrite under the assumption that ferrihydrite has the stoichiometry $Fe(OH)_3$, similar to the gibbsite structure, $Al(OH)_3$. However, assuming the Michel model for ferrihydrite, the appropriate corresponding isostructural Al-oxyhydroxide is akdalaite, Al_5O_8H. The akdalaite standard entropy is estimated by Hemingway et al.[36] as $S°_{akdalaite} = 29.3$ J/(mol-Al K). On the basis of a linear fit of the correlation between entropy values for four isostructural Fe and Al phases (Figure 6), the standard entropy of ferrihydrite is estimated as $S°_{fhyd} = 49.1$ J/(mol-Fe K), or 245.5 J/(mol K) per formula unit Fe_5O_8H.

The Gibbs free energy at 298.15 K of bulk ferrihydrite relative to hematite + water is calculated by the above method to be $\Delta G_{rxm}(Fe_5O_8H) = 6.9$ kJ/(mol-Fe) for $U = 4$ eV (Table 12). The entropic terms for hematite and water were calculated using experimental standard

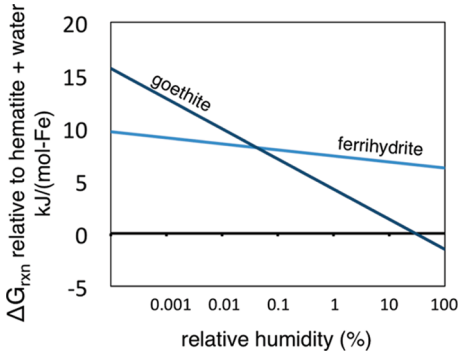

Figure 7. Stability of ferrihydrite and goethite relative to hematite and water vapor versus the logarithm of relative humidity. A crossover stabilizing ferrihydrite relative to goethite is apparent at very low relative humidity (less than 0.1%).

entropy values.[3,33] The Gibbs free energy can also be expressed relative to hematite and water vapor at 298.15 K by noting that H_2O liquid and vapor are in equilibrium at 100% relative humidity (RH), and thus their free energies are equal (e.g., $\mu(H_2O)_{liquid} = \mu(H_2O)_{vapor}$). The Gibbs free energy of ferrihydrite relative to hematite and water vapor at arbitrary RH and $T_0 = 298.15$ K can therefore be obtained from $\Delta G_{rxn}(Fe_5O_8H) = 6.9 - 0.1RT_0 \ln(RH/100) = 6.9 - 0.248 \ln(RH/100)$ kJ/(mol-Fe). Figure 7 shows the calculated stability of ferrihydrite and goethite relative to hematite and water vapor over the full range of relative humidity values, the latter shown in logarithmic scale. It emerges that ferrihydrite becomes stable relative to goethite only at extremely low relative humidity (roughly 0.1% RH). Note that this crossover RH value will change for nanoparticles due to surface energy effects, as discussed in Section IV.D.

D. Effect of Surface Energy on the Stability of Nanoparticle Ferrihydrite. Figure 5 shows that the bulk ferrihydrite relative formation enthalpy is predicted to be well below the experimentally measured value. However, experimental studies of ferrihydrite deal exclusively with nanoparticle samples with high specific surface area; thus, the surface energy contribution must be included before a direct comparison between the experimental and DFT based enthalpies is made. The formation energy of a mineral nanoparticle can be approximately constructed by adding bulk and surface energies. Assuming spherical particles, the particle surface energy is obtained as (eq 11):

$$E_f^{surface}(d) = \Delta H_s^h \cdot 4\pi \left(\frac{d}{2}\right)^2 \qquad (11)$$

where d is the nanoparticle diameter and ΔH_s^h is the effective hydrous surface formation enthalpy (the expression could also be written in terms of the anhydrous surface formation enthalpy, ΔH_s). In this work we will assume a single, constant, effective surface energy. The use of a constant effective surface energy does not take into account a number of factors that can cause changes in the surface energy with diameter, such as changes in bonding strengths, surface reconstructions, defect concentrations, and variations in the fraction with

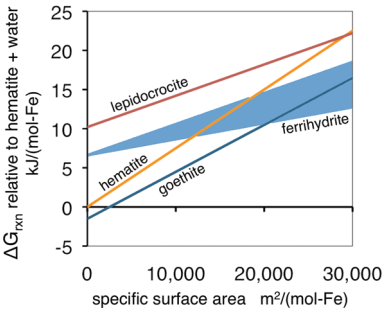

Figure 8. Gibbs free energy of formation relative to bulk hematite and water of nanoparticle Fe-oxyhydroxides as a function of specific surface area. The slope of each line is the hydrated surface formation enthalpy for each oxyhydroxide, as tabulated in ref 3. The *y*-intercepts are the calculated bulk stabilities (Section IV.C). The shaded wedge shows the estimated Gibbs free energy of formation of ferrihydrite, with the hydrated surface energy range estimated based on empirical observations of particle stability and transformation characteristics.

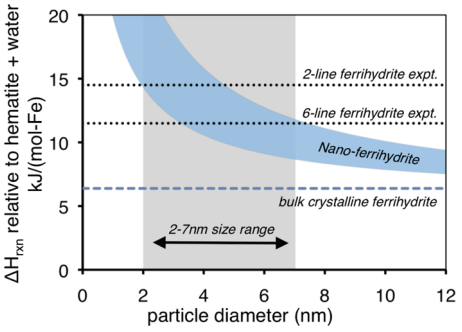

Figure 9. Formation energy model relative to hematite and water for spherical nanoparticles of ferrihydrite (Fhyd) with average surface energy $\Delta H_s^h = 0.2-0.4\ \mathrm{J/m^2}$ (hydrated surface assumed). Experimental reaction enthalpies are shown for 2-line and 6-line nanoparticle samples.[5] On the basis of the DFT energy of undefected bulk crystalline ferrihydrite, destabilization due to positive surface formation energy is of appropriate magnitude to account for the experimentally observed energetics of nanoparticle samples given a realistic distribution of particle sizes from 2 to 7 nm.

which different terminations contribute to the surface morphology, the latter including important effects such as low-coordination corner- and edge sites.[63,64] These effects are likely to become more important for the smallest particles, in the 1−2 nm size range, and a more accurate treatment of the surface energetics may be required in the future for quantitative modeling of the smallest ferrihydrite particles. Both anhydrous and hydrated surface enthalpies for hematite, goethite, lepidocrocite, and other Fe-oxyhydroxides are tabulated in ref 3. Notably absent from the literature is the surface formation energy of ferrihydrite, which is estimated in this section. This paper will focus on the hydrated surface case, as the hydrated surface best represents natural conditions in which mineral precipitations and transformations take place. In all Fe-oxyhydroxide phases, it is found that the hydrated surfaces are stable relative to their anhydrous counterparts in aqueous environments or under typical relative humidity values in air. Hydrated surfaces typically consist of a layer of chemisorbed water molecules overlaid by physisorbed water molecules that behave like bulk water. The chemisorbed water molecules are strongly bound and likely affect surface geometries of the oxyhydroxide and oxide surfaces.[3] The nanoparticle thermodynamic analysis derived here does not explicitly distinguish chemisorbed water from physisorbed water molecules. The thermodynamic analysis of the nanoparticles of the material treat the material in the particle as bulk and water molecules as bulk water, and then the effective surface formation enthalpy term in eq 11 accounts for the changes in energy from these bulk states due to the presence of a surface, chemisorption of surface waters, and surface reconstruction.

The formation energy of a complete nanoparticle can be written as formation energy of the volume of the particle cut from bulk crystalline material, plus the particle surface energy, as shown in eq 12. Surface entropy contributions to the free energy of nanoparticle Fe-oxyhydroxides are not considered in this study; that is, only the enthalpy of surface formation is included.

$$\Delta G_f^{particle}(d) = \Delta G_f^{bulk} \cdot \frac{4\pi}{3}\left(\frac{d}{2}\right)^3 + E_f^{surface}(d) \qquad (12)$$

The surface energy of ferrihydrite is estimated by considering the fairly narrow size range in which ferrihydrite particles are observed (roughly 2−7 nm), and the bulk stability calculated in Section IV.C. To estimate the surface energy of ferrihydrite, we examine Figure 8, which shows the calculated stability, or free energy of formation relative to bulk hematite + water, as a function of surface area (or inversely, particle size), for a number of Fe-oxyhydroxides. The *y*-intercepts of this plot are the calculated bulk stabilities (Section IV.C). The positive slope of each line represents the energy cost of forming 1 m^2 of a hydrated mineral surface per Fe, cut from bulk material. The slope of each solid line comes from experimental data.[3] The surface energy of ferrihydrite is estimated to be within the range of 0.2−0.4 J/m^2. The lower bound is drawn such that ferrihydrite becomes thermodynamically stable relative to goethite at particle sizes smaller than $d = 7$ nm, at a specific surface area (SSA) of roughly 20 000 m^2/(mol-Fe). This bound is based on the fact that ferrihydrite particles larger than ∼7 nm are difficult to obtain or synthesize under normal conditions (e.g., without the incorporation of stabilizing agents such as Si or citrate, which have been shown to aid in the synthesis of ferrihydrite particles larger than 7 nm).[49,65] Ferrihydrite is typically considered to have a low surface formation energy relative to the common Fe-oxyhydroxides;[66] thus, the upper bound of the estimated surface energy range is set to that of lepidocrocite, which has the lowest experimentally measured surface energy (0.4 J/m^2).[3] Proceeding on this basis and drawing conclusions from the lower-bound

(63) Campbell, C. T.; Parker, S. C.; Starr, D. E. *Science* **2002**, *298*(5594), 811–814.
(64) Hummer, D. R.; Kubicki, J. D.; Kent, P. R. C.; Post, J. E.; Heaney, P. J. *J. Phys. Chem. C* **2009**, *113*(11), 4240–4245.
(65) Berquó, T. S.; Banerjee, S. K.; Ford, R. G.; Penn, R. L.; Pichler, T. *J. Geophys. Res.*, [*Solid Earth*] **2007**, *112*(B2), 12.
(66) Waychunas, G. A.; Kim, C. S.; Banfield, J. F. *J. Nanopart. Res.* **2005**, *7*, 409–433.

surface energy, ferrihydrite becomes stable relative to nanoparticle hematite for ferrihydrite particle sizes around d = 10−12 nm, or at a SSA of approximately 12 000 m^2/(mol-Fe).

Figure 9 shows the predicted formation enthalpy of nanoparticle ferrihydrite obtained from eq 12 as a function of particle diameter. The experimental formation enthalpies of 2-line and 6-line ferrihydrite nanoparticles[5] are shown as dotted lines approximately 10−15 kJ/(mol-Fe) above the baseline enthalpy of hematite + water. The lower, dashed line is the DFT formation enthalpy of bulk, crystalline ferrihydrite as calculated in Section IV.C. The curved, shaded region corresponds to the calculated formation enthalpy of spherical ferrihydrite nanoparticles as a function of particle diameter, assuming the estimated surface formation energy range described above. The range of particle formation enthalpies is a consequence of the estimated range of possible surface formation energy values. As the particle diameter decreases, surface formation energy plays a progressively larger role in destabilizing the nanoparticle system relative to the bulk mineral structure. The predicted formation of a ferrihydrite nanoparticle of diameter 4 nm, for instance, ranges from 10 to 15 kJ/(mol-Fe) less stable than bulk hematite and water, consistent with the experimental energetics of nanoparticle ferrihydrite. In the nanoparticle regime, ferrihydrite is the most stable of the modeled Fe-oxyhydroxides for particle sizes below 7 nm, consistent with its observed formation during early stages of Fe-oxyhydroxide nucleation and growth. However, the stability of ferrihydrite at the smallest particle sizes is largely determined by the approximate methods used to fit the ferrihydrite surface energy and cannot be regarded as predictive.

IV. Conclusions

We have perfomed a DFT investigation of the structure, magnetism and relative thermodynamic stability of ferrihydrite and related Fe- and Al-oxyhydroxides. All of the calculations for ferrihydrite are based on the Michel model of the ferrihydrite structure.[1] This model is particularly attractive from a computational standpoint, as it contains a fully periodic, single-phase structure upon which models for more complicated phenomena such as surfaces, defects, and nanoparticles can be built.

The calculations provide structural parameters consistent with those proposed within the Michel model and suggest that the unusual tetrahedral Fe3−O bond lengths found by Michel et al.[1] are not an intrinsic property of the bulk crystalline structure but are instead likely to be due to the compounded influence of surfaces, poor crystallinity, defects, and the structural refinement errors reasonably anticipated for small nanoparticles.

The ground state magnetic ordering for ferrihydrite is predicted by means of a Heisenberg model incorporating exchange couplings fitted to DFT magnetic energetics. A ferrimagnetic ordering is predicted in ferrihydrite, with Fe moments counter-aligning in layers stacked along the c-axis. The ferrimagnetic structure leaves 20% of the Fe moments uncompensated. Monte Carlo simulation of the Heisenberg Hamiltonian places the Néel temperature of bulk ferrihydrite at 250 K, the transition manifesting either second-order or weak first-order character. The magnetic data obtained are in good agreement with the range of experimental Néel temperatures determined experimentally for the Fe-oxyhydroxides, and with the experimental consensus that ferrihydrite should manifest antiferromagnetic coupling, with the presence of some fraction of uncompensated moments. It is likely that nanoparticle ferrihydrite will exhibit considerably more magnetic disorder than the bulk calculations, lowering the net excess moment per atom and possibly lowering the Néel temperature.

It is demonstrated that the DFT thermodynamic model can be made more accurate by the inclusion of an improved description of the correlation effects present in the Fe 3d-electrons, here achieved via the GGA+U method. The best agreement with experimental Fe-oxyhydroxide enthalpy data is achieved for U = 4 eV. Using this U value and assuming the Fe_5O_8H stoichiometry of the Michel model, the formation enthalpy at 298.15 K of bulk crystalline ferrihydrite is calculated to be −435.3 kJ/(mol-Fe) relative to the elements (in their standard state), or 6.4 kJ/(mol-Fe) relative to bulk hematite (α-Fe_2O_3) and liquid water. The Gibbs free energy of formation at 298.15 K is calculated to be ΔG_{rxn} (Fe_5O_8H) = 6.9 kJ/(mol-Fe) relative to hematite (α-Fe_2O_3) and liquid water. Bulk crystalline ferrihydrite is thus metastable relative to goethite and hematite but somewhat more stable than lepidocrocite. Using a hydrous surface formation enthalpy estimate of 0.2−0.4 J/m^2, which is in the lower end of the typical range for Fe-oxides and oxyhydroxides, and the calculated bulk formation enthalpy, hydrated spherical ferrihdyrite particles of diameter 4−5 nm should have a formation enthalpy of roughly 10−15 kJ/(mol-Fe) relative to bulk hematite and water, which is in agreement with published experimental values for 2- and 6-line nanoparticles. The calculated stability of ferrihydrite lends credence to the Michel model, given that an incorrect or inaccurate structure might have led to a significantly higher energy and poorer agreement with the experimental enthalpies. We note that a similar thermodynamic assessment as performed in this work for the Michel model is not applied to other proposed models[8,10−12] for the ferrihydrite structure due to the highly defected, multiphase nature of these models making them particularly challenging for ab initio investigation.

The results support the Michel model as a plausible candidate for the bulk ferrihydrite structure, since our DFT study of the structural, magnetic, and thermodynamic properties of the hypothetical bulk model are in general agreement with experimentally observed properties when the effects due to nanoparticle formation are considered. Assuming that the Michel model is correct, these calculations provide new insights into the atomic, magnetic, and thermodynamic properties of ferrihydrite.

Acknowledgment. We gratefully acknowledge helpful discussions with F. Marc Michel and John Parise. We benefited greatly from the use of Monte Carlo codes developed by Anton Van der Ven, which were modified for the Heisenberg model simulations. We gratefully acknowledge funding support from the National Science Foundation, through a Collaborative Research in Chemistry award, CHE 0714183.

Supporting Information Available: Crystallographic information (CIF). This material is available free of charge via the Internet at http://pubs.acs.org.